Radiation forces of a highly focused radially polarized beam on spherical particles

Shaohui Yan[1,2] and Baoli Yao[1]
[1]*State Key Laboratory of Transient Optics and Photonics, Xi'an Institute of Optics and Precision Mechanics, Chinese Academy of Sciences, Xi'an 710119, China*
[2]*Graduate School of the Chinese Academy of Sciences, Beijing 100039, China*
(Received 11 August 2007; published 29 November 2007)

A radially polarized beam focused by a high-numerical-aperture (NA) objective has a strong longitudinal and nonpropagating electric field in the focal region, which implies that it is suitable for axial optical trapping. In this paper, we use the vectorial diffraction integral to represent the field distribution of the radially polarized beam focused by a high-NA objective and then employ the *T*-matrix method to compute the radiation forces on spherical particles. Effects of different parameters, such as the size of the sphere, the inner radius of the radially polarized beam, and the NA of the objective, on the radiation forces are presented.

DOI: 10.1103/PhysRevA.76.053836 PACS number(s): 42.25.Fx, 87.80.Cc

I. INTRODUCTION

In 1986, Ashkin *et al.* demonstrated that a single focused laser beam can pull up and trap a dielectric microsphere at the position of the focus point [1]. This technology, namely, the optical tweezer, has been widely applied in physics, chemistry, and biophysical studies, e.g., trapping and cooling single molecules and atoms [2], measuring the force associated with the transcription of RNA [3], and moving single DNA molecules in viscous flows [4], and so on. Accurate calculation of the optical forces enables quantitative investigation into the process of interaction between light and matters and a better understanding of the physical mechanism.

The radiation forces exerted by the incident beam on a particle stem from the total momentum change due to scattering, absorption, and emission by the trapped particle. In theory, there are three methods for analysis of optical radiation forces acting on microparticles in terms of the particle's size. If the particle is very small compared with the wavelength of the incident light, the Rayleigh scattering model presents no difficulties for determining the radiation forces on such a small particle [5]. If the size of the particle is much larger than the wavelength of the incident light, the ray optics model can be employed as a good approximation to compute the forces [6]. When the particle's dimension is near the wavelength of the incident light, these two models fail to offer an adequate solution to the problem considered. In this case, the radiation force is obtained via the Maxwell stress tensor, which requires knowledge of the scattered field outside the particle. For spherical particles, the Mie scattering theory can provide an exact solution to the scattering field; then the radiation force on the sphere is determined by integrating the Maxwell stress tensor over a spherical surface at infinity. A comprehensive overview of how to calculate the radiation on the sphere using the generalized Lorenz-Mie theory has been made by Lock [7]. Recently, the *T*-matrix method has also been applied to the calculation of radiation forces acting on particles [8–12]. Since the *T*-matrix method can compute the field scattered by a nonspherical particle, it is able to obtain the radiation forces on spheroidal and even ellipsoidal particles [13,14].

Generally, we employ a fundamental mode Gaussian beam to represent the incident field near the focus after being focused by an objective. This description for the field, however, has non-negligible error, especially in the case of a beam focused by a high-numerical-aperture (NA) objective. A fifth-order corrected Gaussian model has been proposed by Barton and Alexander to diminish the error [15]. Another alternative to modeling the incident beam is the so-called vectorial diffraction theory, which is based on the vectorial Debye-type integral formulated by Wolf and Richards in their classical paper [16]. Relative to the fifth-order corrected Gaussian model, the vectorial diffraction theory can deal with the effect of diffraction by a high-NA objective, the apodization function, and spherical aberration. It thus correctly characterizes the field distribution near the focus.

By now, linearly or circularly polarized beams are the most common ones used in optical trapping. Recently, beams with cylindrically symmetric polarization such as radial polarization have been widely studied. Many methods have been proposed for generating a radially polarized beam and the properties of the beam have been analyzed in detail [17–22]. The polarization property of the radial polarization field causes it to have a vanishing Poynting flux component along the propagation axis near the focus under tightly focusing conditions [21,22]. This character implies that the radial polarization field may reduce the scattering force and thus improve the axial trapping efficiency. Zhan [22] demonstrated this possibility for a metallic Rayleigh particle. Kawauchi *et al.* [23] showed that higher axial trapping efficiency is obtained by using a radially polarized beam to illuminate a dielectric particle in the ray optics regime.

In this paper, we use the *T*-matrix method to calculate radiation forces on more general dielectric particles with size ranging from the Rayleigh regime to several wavelengths, illuminated by a radially polarized beam focused by a high-NA objective. A familiar calculation for such general particles with linear polarization beams has been done by Ganic *et al.* [24,25]. We use a Debye-type integral to describe the field distribution near the focus. For each angular spectrum of plane waves in the integrand, the expansion coefficients of vector spherical wave functions (VSWFs) can be easily obtained. The expansion coefficients of the total field are thus integrals of those of each of the plane waves. Once the expansion coefficients of the incident field is known, the scattering field is obtained by means of the *T* matrix, and the

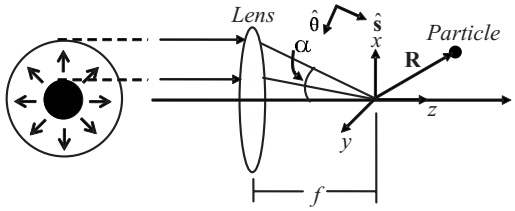

FIG. 1. Geometry of a particle trapped by a radially polarized beam focused by a lens. α is the maximum convergence angle given by the lens, f is the focal length, $\hat{\mathbf{s}}$ and $\hat{\boldsymbol{\theta}}$ denote the wave vector direction of a given plane wave spectrum and its polarization direction, respectively, and $\mathbf{R}$ is the position of the trapped particle.

radiation forces are computed via the Maxwell stress tensor. Numerical calculations of the radiation forces on spherical particles exerted by the radial polarization field with different configurations, such as the numerical aperture and the inner radius of the beam, are given. At the same time, the case of a linear polarization field is also discussed as a comparison.

II. THEORETICAL MODELING

Generally, there are two types of methods for obtaining a radially polarized beam. One type generates the beam outside the laser cavity, e.g., Shoham *et al.* [18] used two conical reflectors and a cylindrical sheet of polarizing film to produce a radially polarized beam from a randomly polarized source. The other type generates the beam inside the laser cavity, for example, Kozawa and Sato [19] placed two conical prisms, one convex and the other concave, inside a neodymium-doped yttrium aluminum garnet (Nd:YAG) laser cavity to obtain an output of the radially polarized TEM_{01} mode. The polarization of such a beam is in the radial direction, and the intensity distribution is of cylindrical symmetry and takes on a ring shape as shown in Fig. 1. The radially polarized beam focused by a high-NA objective has a strong longitudinal and nonpropagating electric field in the focal region [21,22]. For this field near the focus to be suited to the T-matrix method, we first need to analyze the VSWF expansions of the radially polarized beam in the focal region.

A. Expansion of a radially polarized beam using vector spherical wave functions

The geometry of a radial polarization beam focused by an objective is illustrated in Fig. 1. A radially polarized beam with a planar wave front propagates along the optical axis from the left and is focused by an aplanatic lens to produce a converging spherical wave toward the focus of the lens. The particle to be trapped is located somewhere near the focus. For convenience of calculation, we set the focus point as the origin of the coordinate system and denote the center position of the sphere by the vector $\mathbf{R}$. The refractive indices of the particle and the environment are, respectively, n_2 and n_1.

According to the Debye-type integral representation developed by Wolf and Richards [16], the electric field of the radially polarized beam focused by a high-NA objective can be written as

$$\mathbf{E}^i(\mathbf{r}) = \frac{-ikf}{2\pi}\int_0^{\alpha}\int_0^{2\pi} \sin\theta(\cos\theta)^{1/2} l(\theta) \times \exp[ik\hat{\mathbf{s}}\cdot(\mathbf{r}-\mathbf{R})]\hat{\boldsymbol{\theta}}\, d\phi\, d\theta, \tag{1}$$

in which k and f are the wave number in the ambient medium and the focal length of the lens, respectively, α is the maximal angle give by the NA of the objective lens, and $l(\theta)$ stands for the amplitude of the field at the entrance pupil of the lens, which has a cylindrical symmetry about the optical axis. The vector $\mathbf{r}$ designates the observation point position, and the unit vector $\hat{\mathbf{s}}(\theta,\ \phi)$ defines the wave vector direction of a given plane wave, where $(\theta,\ \phi)$ represent the polar and azimuthal angles, respectively, in a spherical coordinate system. The polarization direction of the field in image space is described by the unit vector $\hat{\boldsymbol{\theta}}$ in the θ direction.

In the T-matrix method, all the fields are expanded in terms of vector spherical wave functions,

$$\mathbf{E}^i(\mathbf{r}) = \sum_{n=1}^{\infty}\sum_{m=-n}^{n}[a_{mn}\mathbf{M}_{mn}^1(k\mathbf{r}) + b_{mn}\mathbf{N}_{mn}^1(k\mathbf{r})], \tag{2a}$$

$$\mathbf{E}^s(\mathbf{r}) = \sum_{n=1}^{\infty}\sum_{m=-n}^{n}[e_{mn}\mathbf{M}_{mn}^3(k\mathbf{r}) + f_{mn}\mathbf{N}_{mn}^3(k\mathbf{r})], \tag{2b}$$

where $\mathbf{M}_{mn}^{1,3}(k\mathbf{r})$ and $\mathbf{N}_{mn}^{1,3}(k\mathbf{r})$ are VSWFs of the first and third kind [26], and the expansion coefficients a_{mn} and b_{mn} of the incident field can be determined from Eq. (1). In Eq. (1), the incident field is a superposition of a series of plane waves with polarization in the θ direction. For each plane wave component, we have the following expansions [26]:

$$(\cos\theta)^{1/2} l(\theta)\exp(ik\hat{\mathbf{s}}\cdot\mathbf{r})\hat{\boldsymbol{\theta}} = \sum_{n=1}^{\infty}\sum_{m=-n}^{n}[A_{mn}\mathbf{M}_{mn}^1(k\mathbf{r}) + B_{mn}\mathbf{N}_{mn}^1(k\mathbf{r})], \tag{3}$$

with

$$\begin{bmatrix} A_{mn} \\ B_{mn} \end{bmatrix} = (-4i^{n+1})\pi(\cos\theta)^{1/2} l(\theta)\begin{bmatrix} m\Pi_n^m(\theta)e^{-im\phi} \\ \tau_n^m(\theta)e^{-im\phi} \end{bmatrix}, \tag{4}$$

where $\Pi_n^m(\theta)$ and $\tau_n^m(\theta)$ are functions involving the associated Legendre functions. Substituting this expression into Eq. (1) and using the integral representation of the cylindrical Bessel function, we finally have

$$a_{mn} = -8\pi(mi^{n+1-m}e^{-im\phi_0}) \times \int_0^{\alpha}(\cos\theta)^{1/2} l(\theta)\Pi_n^3(\theta)J_m(k\rho_0\sin\theta) \times \exp(-ikz_0\cos\theta)\sin\theta\, d\theta, \tag{5a}$$

$$b_{mn} = -8\pi(i^{n+1-m}e^{-im\phi_0}) \times \int_0^{\alpha}(\cos\theta)^{1/2} l(\theta)\tau_n^m(\theta)J_m(k\rho_0\sin\theta) \times \exp(-ikz_0\cos\theta)\sin\theta\, d\theta, \tag{5b}$$

in which (ρ_0, ϕ_0, z_0) denote the position of the center of the sphere and $J_m(x)$ is the cylindrical Bessel function of order m.

B. Radiation forces

Knowing the expansion coefficients of the incident field, we can easily obtain the expansion coefficients of the scattered field by use of the T matrix

$$\begin{bmatrix} e_{mn} \\ f_{mn} \end{bmatrix} = \begin{bmatrix} T^{11}_{mnm'n'} & T^{12}_{mnm'n'} \\ T^{21}_{mnm'n'} & T^{22}_{mnm'n'} \end{bmatrix} \begin{bmatrix} a_{m'n'} \\ b_{m'n'} \end{bmatrix}, \tag{6}$$

where $[T]$ is the T matrix related to the particle [26].

The radiation force is computed by integrating the Maxwell stress tensor over any closed surface surrounding the particle (for simplicity, we choose a sphere at infinity):

$$\langle \mathbf{F} \rangle = \lim_{r\to\infty} \left(-\frac{1}{2} r^2 \int_{4\pi} d\Omega\, \mathbf{n} (\varepsilon E^2 + \mu_0 H^2) \right), \tag{7}$$

in which E and H are the amplitudes of the total electric and magnetic fields,

$$E = |\mathbf{E}^i + \mathbf{E}^s|, \quad H = |\mathbf{H}^i + \mathbf{H}^s|. \tag{8}$$

With the expansion of fields Eq. (1) substituted into Eq. (7), we can express the force in terms of the coefficients of the field,

$$\langle F_z \rangle = -\frac{\varepsilon}{2k^2} \sum_{n=1}^{\infty} \sum_{m=-n}^{n} \mathrm{Im} \left(\frac{1}{(n+1)} \sqrt{\frac{n(n+2)(n-m+1)(n+m+1)}{(2n+1)(2n+3)}} (2e^*_{n+1,m} e_{n,m} + 2f^*_{n+1,m} f_{n,m} + e^*_{n+1,m} a_{n,m} + a^*_{n+1,m} e_{n,m} \right.$$
$$\left. + f^*_{n+1,m} b_{n,m} + b^*_{n+1,m} f_{n,m}) + \frac{m}{n(n+1)} i (2 f_{n,m} e^*_{n,m} + e_{n,m} b^*_{n,m} + a_{n,m} f^*_{n,m}) \right), \tag{9}$$

where ε is the permittivity of the medium outside the particle. The more complex transverse force expressions can be found in Refs. [14]. More generally, we use the dimensionless force, the trapping efficiency, which is given by

$$Q_i = \frac{F_i}{(n_1 P/c)}, \quad i = x, y, z, \tag{10}$$

where P is the incident beam power and c is the speed of light in free space. F_i are calculated from Eq. (9). Q_i quantifies how efficiently the available field momentum is transferred to the particle and does not depend on the power P [5–7]. Alternatively, we also use the three-dimensional trapping efficiency $\mathbf{Q}$, whose three components are given by Eq. (10).

III. NUMERICAL RESULTS AND DISCUSSION

Traditionally, we divide the radiation force into two parts: the gradient and scattering forces. The gradient force is related to the gradient of the modulus squared of the incident field, $|\mathbf{E}^i|^2$, and for Rayleigh particles it is proportional to the gradient of $|\mathbf{E}^i|^2$ [5]. The scattering force is always along the propagation direction of the incident beam (commonly the z axis), and a strong longitudinal Poynting vector component leads to a strong scattering force [5,6], which is the situation of the linearly polarized field. Meanwhile, a large particle size gives a large scattering force, since a large size means that the particle can absorb more photons when interacting with the incident beam, which thus results in a larger scattering force [6]. Because the radially polarized field has avanishing longitudinal Poynting vector component near the focus, we may expect the radially polarized field to provide higher axial trapping efficiency by reducing the scattering force. However, for Rayleigh particles, the scattering force is not obvious [5], since they have very small interacting surfaces with the incident beam. So the significant improvement occurs when the size of the particle is of the order of the wavelength. This will be clearly revealed below.

Now we present some numerical results to see how the radially polarized beam affects the radiation forces. Throughout this paper, we set the refractive index of the particle as $n_2 = 1.59$, and that of the medium as $n_1 = 1.33$. The wavelength of the incident beam is assumed to be $\lambda_0 = 1.064$ μm in free space, and the pupil apodization function of the incidence has a simple form as in Ref. [22]:

$$l(\theta) = \begin{cases} l_0, & \sin^{-1}(\mathcal{A}_1) \le \theta \le \sin^{-1}(\mathcal{A}/n_1), \\ 0 & \text{otherwise}, \end{cases} \tag{11}$$

where l_0 is a constant factor dependent on the power of the incident field and $\mathcal{A}$ is the numerical aperture of the lens. $\mathcal{A}_1$ corresponds to the inner radius of the annulus, which is variable.

First of all, we examine the case of Rayleigh particles which correspond to very small particles. Figure 2 presents trapping efficiencies of a sphere with radius $a = 50$ nm illuminated by a radial polarization beam, where the transverse trapping is assumed to be along the x axis in the focal plane and the axial trapping means that the particle moves only along the z axis. As a comparison, the trapping efficiency of a linearly polarized (x direction) plane wave, which uniformly fills the entrance pupil of the objective, is also plotted (dashed line). Here, we choose $\mathcal{A} = 1.26$, and for the radial

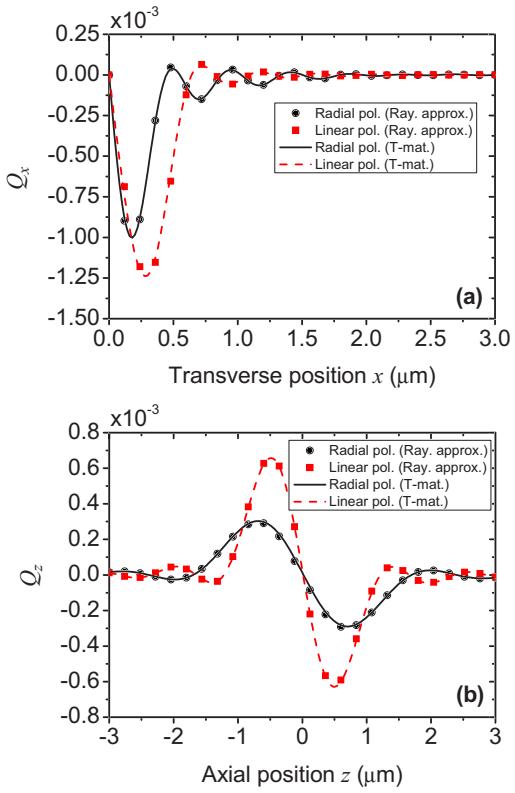

FIG. 2. (Color online) Trapping efficiency **Q** of a Rayleigh sphere (a=50 nm) as a function of the position of the sphere. $\mathcal{A}$ =1.26 and $\mathcal{A}_1$=0.6 for the radial polarization beam. (a) Transverse trapping efficiency along the x axis; (b) axial trapping efficiency.

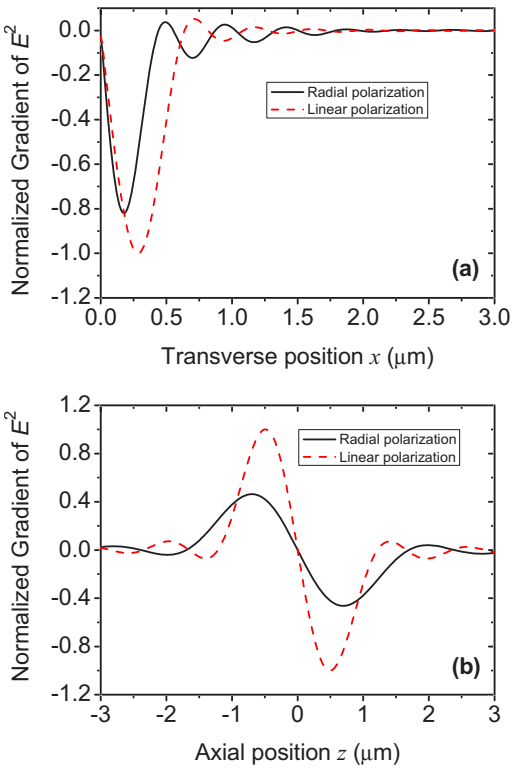

FIG. 3. (Color online) Comparison of the gradient of modulus squared of E (incident electric field) for radial and linear polarization modes with $\mathcal{A}$=1.26 and for the radial polarization $\mathcal{A}_1$=0.6. The values are normalized by the maximum of the linear polarization mode. Component along (a) x and (b) z axis.

polarization beam $\mathcal{A}_1$=0.6. To justify our T-matrix method, we use the Rayleigh model [5] to calculate the trapping efficiencies for both radial and linear polarization (solid symbols). It can be easily seen that for such a small particle the two methods can reach very good agreement for either transverse or axial trapping forces. From Fig. 2, we see that the maximal trapping efficiencies produced by the radial polarization beam are less than those of the linear polarization plane wave for both Q_x and Q_z. This difference lies in the fact that in the Rayleigh regime the dominant term of the radiation forces of a very small particle ($ka \ll 1$) is proportional to the gradient of $|\mathbf{E}^i|^2$. To illustrate this, a comparison of the gradient of $|\mathbf{E}^i|^2$ for the radial and linear polarization modes is plotted in Fig. 3, in which the values are normalized by the maximum of the linear polarization mode. We see clearly that the linear polarization plane wave has larger gradients of $|\mathbf{E}^i|^2$ in both the x and z directions, which determines that the trapping efficiencies related to the two polarization modes must have the same trend as shown in Fig. 2.

Now we turn to the case of a large particle (a ~wavelength λ). In Fig. 4, we compute the radiation forces on a spherical particle of radius a=1 μm with a radially and a linearly polarizated beam, respectively. We find that for a spherical particle with size of the order of the wavelength, the transverse radiation force given by the linearly polarized plane is still larger than that produced by the radially polarizated beam, which is in accordance with what we see in the Rayleigh case above, but the difference in magnitude is increased. However, in contrast to Fig. 2(b), the radial polarization beam gives rise to greater backward axial trapping force as seen in Fig. 4(b). This phenomenon occurs because the radial polarization beam has a vanishing component of the Poynting vector along the axial direction, which surely lowers the so-called scattering forces on the particle.

For a comprehensive examination of the effects of the two types of polarization field on particles, a comparison of maximal trapping efficiencies $Q_{\max}$ between the radial and linear polarization beams with varying size of the sphere is presented in Fig. 5. As we see, the maxima of both Q_x and Q_z increase with increasing size of the sphere. When the sphere is large enough (about 1 μm), gentle increases appear, which implies that the results are approaching the geometric optics prediction, where the trapping forces are independent of the size of the sphere. In Fig. 5, we note that the radiation forces of radial polarization and linear polarization present different variation trends. For the transverse $Q_{\max}$, the linear polarization field corresponds to larger values than the radial polarization field in both small and large size ranges. With increasing size, the gap becomes more obvious, e.g., at a =0.05 μm, the transverse $Q_{\max}$ corresponding to the linear and radial modes are 0.0012 and 0.0010 with the ratio equal to 1.2, while at a=0.5 μm, the ratio becomes 1.91. For the axial $Q_{\max}$, the situation is different. With a radius less than some size (between 0.5 and 0.6 μm), the linear polarization shows greater values. But for large size, the radial polarization field exhibits values much larger than those corre-

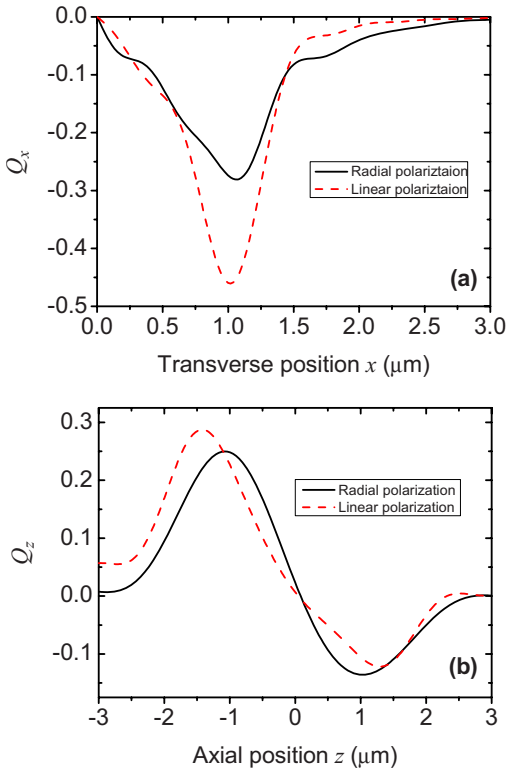

FIG. 4. (Color online) Trapping efficiency **Q** of a sphere ($a=1$ μm) as a function of the position of the sphere. $\mathcal{A}=1.26$ and $\mathcal{A}_1=0.6$ for the radial polarization beam. (a) Transverse trapping efficiency along the x axis; (b) axial trapping efficiency.

sponding to the linear polarization field. When $a=3$ μm, for example, the axial $Q_{\max}$ corresponding to the radial and linear polarization fields is, respectively, 0.1860 and 0.1134, and their ratio is up to 1.64. Obviously, this results directly from the fact that the radial polarization field has a zero axial component of the Poynting vector near the focus, as we pointed out in the analysis of Fig. 2. Meanwhile, the trend of the axial $Q_{\max}$ curve implies that even for particles in the ray optics regime ($a>5$ μm). This property of the radial polarization field may be used to improve the axial trapping efficiency for large-size particles.

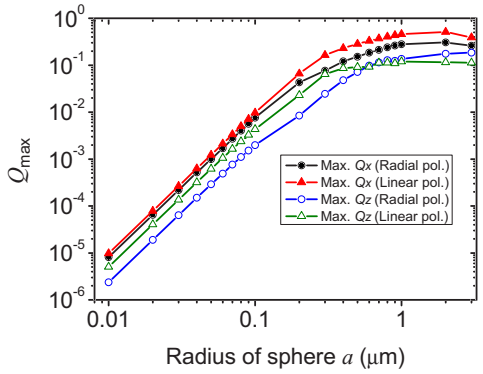

FIG. 5. (Color online) Comparison of $\mathbf{Q}_{\max}$ between the radial polarization beam and the linear polarization beam as a function of the sphere radius $a(0.01\sim3$ μm). $\mathcal{A}=1.26$ and $\mathcal{A}_1=0.6$ for the radial polarization beam.

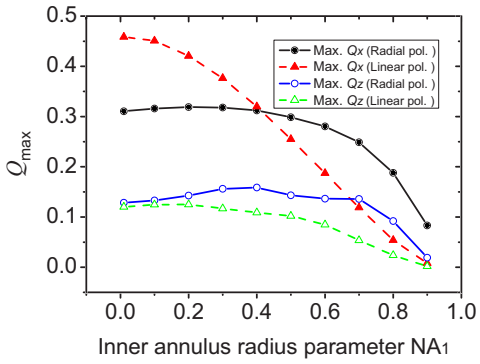

FIG. 6. (Color online) Maximal trapping efficiencies $\mathbf{Q}_{\max}$ in transverse and axial directions of a sphere of radius $a=1$ μm with different $\mathcal{A}_1$ ($\mathcal{A}=1.26$) for both radial and linear polarization beams.

In all preceding calculations, the inner radius of the annulus $\mathcal{A}_1$ for the radial polarization is set equal to 0.6. At the beginning of this section, we stated that this value is variable. We may expect some changing results for the radiation forces on varying the size of the inner radius. In Fig. 6, we plot the curves of the maximal trapping efficiencies $Q_{\max}$ as $\mathcal{A}_1$ varies. As a comparison, the change in inner radius of the annulus for the linear polarization plane wave is realized by obstructing the beam with an opaque disk [24]. We center our discussion on a spherical particle with radius $a=1$ μm and the numerical aperture of the objective, $\mathcal{A}$, is still equal to 1.26. We see from Fig. 6 that both the transverse and the axial $Q_{\max}$ corresponding to the linear polarization plane wave decrease as $\mathcal{A}_1$ increases (i.e., with increasing obstruction size). Especially for the transverse $Q_{\max}$, the drop is very obvious, and the trend is in good agreement with the result of Fig. 1 in Ref. [24]**.** However, for the radial polarization mode, both the transverse and the axial $Q_{\max}$ first go up and then decline with increasing value of $\mathcal{A}_1$; when $\mathcal{A}_1$ is about 0.4, the largest value for the axial $Q_{\max}$ appears, and the largest value for the transverse $Q_{\max}$ emerges when $\mathcal{A}_1$ is roughly equal to 0.2. Note that the value of the transverse $Q_{\max}$ at $\mathcal{A}_1=0.4$ is just slightly smaller than the transverse $Q_{\max}$ at $\mathcal{A}_1=0.2$, so, taking $\mathcal{A}_1=0.4$ is a good solution from all points of view.

Finally, the effect of the numerical aperture of the objective lens on the radiation forces for the radial polarization beam is examined. In our consideration, we fix the ratio of inner and outer radii of the radial polarization beam at $0.6/0.95=0.63$. According to Fig. 7, as the NA increases, either the transverse or the axial $Q_{\max}$ increases.

IV. CONCLUSIONS

Based on the vectorial diffraction theory and T-matrix method, we have presented the radiation forces of the radial and linear polarization beams on dielectric particles with size ranging from the Rayleigh regime to several wavelengths. For Rayleigh particles, our calculation results are in good agreement with those predicted by the Rayleigh scattering model. These results show that the linear polarization mode

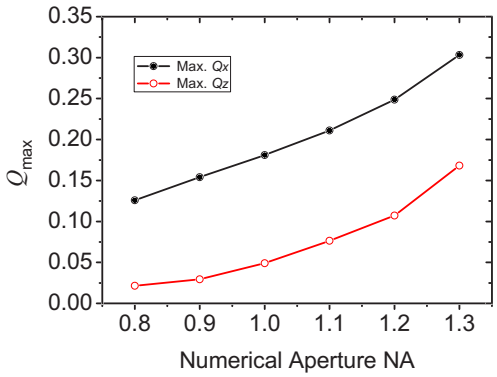

FIG. 7. (Color online) Maximal trapping efficiencies $\mathbf{Q}_{max}$ of a sphere of radius $a=1$ μm versus the objective NA, with the fixed ratio 0.63 of the inner and outer radii of the radial polarization beam.

can provide larger gradient forces in both transverse and axial radial directions compared to a radial polarization field. Since the scattering force for Rayleigh particles is small due to their small size, the net trapping force given by the linearly polarized field is also larger. When the size of the particles approaches the wavelength of the beam, the scattering force becomes obvious. Benefiting from the vanishing axial component of the Poynting vector near the focus, the radial polarization field improves the axial trapping efficiency by reducing the scattering force. With increasing size of the particles, this improvement also increases. The calculation indicates that, even for larger particles in the ray optics regime, the improvement still exists, which was also tested by other authors' work [23]. Meanwhile the trapping efficiency can be changed by adjusting the configuration of the beam. With increasing inner radius of the radial polarization beam, the axial trapping efficiency increases before reaching a maximum, and then decreases, while the transverse trapping efficiency gently decreases in a large zone at the beginning. Thereby an optimal inner radius can be taken for obtaining both good axial and good transverse trapping efficiencies. When the numerical aperture of the objective lens is increased, the trapping efficiencies simply increase. These calculation results provide a suggestive reference for design of efficient optical trapping devices.

[1] A. Ashkin, J. M. Dziedzic, J. E. Bjorkholm, and S. Chu, Opt. Lett. **11**, 288 (1986).
[2] S. Chu, Rev. Mod. Phys. **70**, 685 (1998).
[3] H. Yin, M. D. Wang, K. Svoboda, R. Landick, S. M. Block, and J. Gelles, Science **270**, 1653 (1995).
[4] T. T. Perkins, D. E. Smith, R. G. Larson, and S. Chu, Science **268**, 83 (1995).
[5] Y. Harada and T. Asakura, Opt. Commun. **124**, 529 (1996).
[6] A. Ashkin, Biophys. J. **61**, 569 (1992).
[7] J. A. Lock, Appl. Opt. **43**, 2545 (2004).
[8] T. A. Nieminen, N. R. Heckenberg, and H. Rubinsztein-Dunlop, Proc. SPIE **5514**, 514 (2004).
[9] S. Bayoudh, T. A. Nieminen, N. R. Heckenberg, and H. Rubinsztein-Dunlop, J. Mod. Opt. **50**, 1581 (2003).
[10] T. A. Nieminen, H. Rubinsztein-Dunlop, N. R. Heckenberg, and A. I. Bishop, Comput. Phys. Commun. **142**, 468 (2001).
[11] A. I. Bishop, T. A. Nieminen, N. R. Heckenberg, and H. Rubinsztein-Dunlop, Phys. Rev. A **68**, 033802 (2003).
[12] W. Singer, T. A. Nieminen, U. J. Gibson, N. R. Heckenberg, and H. Rubinsztein-Dunlop, Phys. Rev. E **73**, 021911 (2006).
[13] S. H. Simpson and S. Hanna, J. Opt. Soc. Am. A **24**, 430 (2007).
[14] S. Yan and B. Yao, J. Opt. Soc. Am. B **24**, 1596 (2007).
[15] J. P. Barton and D. R. Alexander, J. Appl. Phys. **66**, 2800 (1989).
[16] B. Richards and E. Wolf, Proc. R. Soc. London, Ser. A **253**, 358 (1959).
[17] R. Dorn, S. Quabis, and G. Leuchs, Phys. Rev. Lett. **91**, 233901 (2003).
[18] A. Shoham, R. Vander, and S. G. Lipson, Opt. Lett. **31**, 3405 (2006).
[19] Y. Kozawa and S. Sato, Opt. Lett. **30**, 3603 (2005).
[20] G. Machavariani, Y. Lumer, I. Moshe, A. Meir, and S. Jackel, Opt. Lett. **32**, 1468 (2007).
[21] K. S. Youngworth and T. G. Brown, Opt. Express **7**, 77 (2000).
[22] Q. Zhan, Opt. Express **12**, 3377 (2004).
[23] H. Kawauchi, K. Yonezawa, Y. Kozawa, and S. Sato, Opt. Lett. **32**, 1839 (2007).
[24] D. Ganic, X. Gan, and M. Gu, Opt. Express **12**, 2670 (2004).
[25] D. Ganic, X. Gan, and M. Gu, Opt. Express **13**, 1260 (2005).
[26] M. I. Mishchenko, L. D. Travis, and A. A. Lacis, *Scattering, Absorption, and Emission of Light by Small Particles* (Cambridge University Press, Cambridge, U.K., 2002).